

EARLY-TYPE GALAXIES IN THE PEARS SURVEY:  
PROBING THE STELLAR POPULATIONS AT MODERATE REDSHIFT

IGNACIO FERRERAS<sup>1,2</sup>, ANNA PASQUALI<sup>3</sup>, SANGEETA MALHOTRA<sup>4</sup>, JAMES RHOADS<sup>4</sup>, SETH COHEN<sup>4</sup>, ROGIER WINDHORST<sup>4</sup>,  
NOR PIRZKAL<sup>5</sup>, NORMAN GROGIN<sup>5</sup>, ANTON M. KOEKEMOER<sup>5</sup>, THORSTEN LISKER<sup>6</sup>, NINO PANAGIA<sup>5</sup>, EMANUELE DADDI<sup>7</sup>,  
NIMISH P. HATHI<sup>8</sup>

*Submitted for publication in The Astrophysical Journal*

ABSTRACT

Using *HST*/ACS slitless grism spectra from the PEARS program, we study the stellar populations of morphologically selected early-type galaxies in the GOODS North and South fields. The sample – extracted from a visual classification of the (v2.0) *HST*/ACS images and restricted to redshifts  $z > 0.4$  – comprises 228 galaxies ( $i_{F775W} < 24$  mag, AB) out to  $z \lesssim 1.3$  over  $320 \text{ arcmin}^2$ , with a median redshift  $z_M = 0.75$ . This work significantly increases our previous sample from the GRAPES survey in the HUDF (18 galaxies over  $\sim 11 \text{ arcmin}^2$ ; Pasquali et al. 2006b). The grism data allow us to separate the sample into ‘red’ and ‘blue’ spectra, with the latter comprising 15% of the total. Three different grids of models parameterising the star formation history are used to fit the low-resolution spectra. Over the redshift range of the sample – corresponding to a cosmic age between 5 and 10 Gyr – we find a strong correlation between stellar mass and average age, whereas the *spread* of ages (defined by the RMS of the distribution) is roughly  $\sim 1$  Gyr and independent of stellar mass. The best-fit parameters suggest it is formation epoch and not formation timescale, that best correlates with mass in early-type galaxies. This result – along with the recently observed lack of evolution of the number density of massive galaxies – motivates the need for a channel of (massive) galaxy formation bypassing any phase in the blue cloud, as suggested by the simulations of Dekel et al. (2009).

*Subject headings:* galaxies: elliptical and lenticular, cD - galaxies: evolution - galaxies: stellar content

1. INTRODUCTION

For nearly a century, we have known that the local galaxy population follows a bimodal colour distribution, with a majority of star-forming galaxies and a minority of early-type systems (Hubble 1926; Strateva et al. 2001; Blanton et al. 2003). This distribution (which has been observed up to  $z \sim 1$ , Bell et al. 2004) is commonly interpreted as the outcome of different star-formation histories, with blue galaxies undergoing a much more prolonged star-formation activity than the early-types. This does not rule out that early-type galaxies may also experience occasional episodes of star formation at  $z \sim 0$ . However, if they do, they produce an amount (in mass) of young stars definitively lower than the blue-peak galaxies (Trager et al. 2000; Ferreras et al. 2006; Rogers et al. 2007). Early-type galaxies are known to exhibit a tight colour-magnitude relation (up to  $z \lesssim 1$ , Stanford et al. 1998) which is the direct result of a metallicity sequence where more massive galaxies are also metal-richer (Bower et al. 1992; Kodama & Arimoto 1997; Vazdekis

et al. 2001; Bernardi et al. 2003). The small scatter in their colours and mass-to-light ratios (see e.g. Kelson et al. 2000), and their relatively high  $[\alpha/\text{Fe}]$  (Nelán et al. 2005; Thomas et al. 2005) suggest that early-type galaxies formed the bulk of their stars at high redshift ( $z \gtrsim 3$  van Dokkum et al. 1998; Thomas et al. 2005) and on a relatively short timescale (i.e.  $\sim 1$  Gyr for the more massive galaxies, Thomas et al. 1999). While these properties can be well reproduced by the “monolithic collapse hypothesis” (Eggen et al. 1962; Larson 1974), this scenario does not fit well within the currently accepted  $\Lambda$ CDM galaxy formation paradigm, in which galaxies form through hierarchical buildup. In semi-analytical models, the hierarchical growth of dark matter structures is complemented by the addition of simple prescriptions of the baryonic physics which describe star formation, chemical enrichment, stellar and AGN feedback (e.g. Scannapieco et al. 2005; Croton et al. 2006; Hopkins et al. 2006; Monaco et al. 2007; Hopkins et al. 2008; Somerville et al. 2008). The model predictions are in reasonable agreement with the observed properties of early-type galaxies (see e.g. Kaviraj et al. 2005; De Lucia et al. 2006; Khochfar & Silk 2006a,b), but they still can not reproduce the observed high  $[\alpha/\text{Fe}]$  ratios. On the other hand, support to the merging scenario is given by the detection, at rest-frame UV wavelengths, of recent episodes of star formation in early-type galaxies (Ferreras & Silk 2000; Kaviraj et al. 2007; Rogers et al. 2007; Schawinski et al. 2007; Kaviraj et al. 2008) and by the evidence that less massive early-type galaxies increased their mass by 20 – 40% since  $z=1$  (Bell et al. 2004; Ferreras et al. 2005; Treu et al. 2005a).

We note that all the knowledge collected on early-types is primarily based on the nearby galaxy population. Ex-

<sup>1</sup> ferreras@star.ucl.ac.uk

<sup>2</sup> Mullard Space Science Laboratory, University College London, Holmbury St Mary, Dorking, Surrey RH5 6NT, UK.

<sup>3</sup> Max-Planck-Institut für Astronomie, Königstuhl 17, D-69117 Heidelberg, Germany

<sup>4</sup> Department of Physics and Astronomy, Arizona State University, P.O. Box 871504, Tempe, AZ 85287-1504

<sup>5</sup> Space Telescope Science Institute, 3700 San Martin Drive, Baltimore, MD 21218

<sup>6</sup> Astronomisches Rechen-Institut, Zentrum für Astronomie, Universität Heidelberg, Mönchhofstr. 12-14, D-69120 Heidelberg, Germany

<sup>7</sup> CEA Saclay, Orme des Merisiers, 91191 Gif-sur-Yvette Cedex, France

<sup>8</sup> Department of Physics and Astronomy, University of California, Riverside, CA 92521

tending the study to a large number of early-type galaxies at intermediate and high redshifts allows us to trace their mass-assembly and star formation histories in great detail and, consequently, to fine-tune the theory of galaxy formation and evolution. Ferreras et al. (2009a,b) derived the evolution of number density and size (i.e. half light radius) for a sample of early-type galaxies between  $z=1$  and  $z=0$ , extracted from the GOODS North and South fields (see also Ferreras et al. 2005) and compared it with recent surveys such as GOODS/MUSIC (Fontana et al. 2006), DEEP2 (Conselice et al. 2007; Trujillo et al. 2007), COMBO17 Borch et al. (2006), 2dFGRS (Croton et al. 2005) and SDSS (Shen et al. 2003). They found that massive early-types do not exhibit any significant change in comoving number density over the past 8 billion years. On the contrary, there exists a noticeable evolution in size, implying an increase of about a factor of 2 for early-type galaxies more massive than  $10^{11}M_{\odot}$  and a factor of  $\sim 50\%$  for the less massive ones. This result is in agreement with Daddi et al. (2005), Conselice et al. (2007), Trujillo et al. (2006,2007), Scarlata et al. (2007), van Dokkum et al. (2008) and van der Wel et al. (2008). The latter also found that the  $\sigma$ - $R_e$  relation is different for nearby and distant early-type galaxies, suggesting a significant change in the dynamics of these galaxies. Given the exposure times needed for accurate velocity dispersions in these galaxies, it does not come as a surprise that the amount of evolution of the velocity dispersion is still controversial (see e.g. Cenarro & Trujillo 2009; van Dokkum et al. 2009; Cappellari et al. 2009). Comparison with the semi-analytical models of Khochfar & Silk (2006a,b) – where galaxy growth occurs via dissipative major mergers – suggests that the constant comoving number density at high  $M_*$  is due to a balance between the “sink” (i.e. loss due to mergers of massive galaxies producing more massive galaxies) and the “source” terms (i.e. gain from mergers at lower mass) in the  $0 < z < 1$  range. Ferreras et al. (2009a) also showed that the slope of the Kormendy relation in the  $0.4 < z < 1.4$  range is consistent with  $z=0$  values (see also Ziegler et al. 1999; Waddington et al. 2002). Only the average surface brightness is seen to change, according to pure passive evolution of old stellar populations.

The fact that stellar populations in early-type galaxies undergo passive evolution is confirmed by their colours and photometric spectral energy distributions (SEDs). Morphologically-selected early-type galaxies have been so far identified in clusters up to  $z \simeq 1.4$  and their colours have been proven to be consistent with those of  $z=0$  early-types through pure passive evolution of their stars (see e.g. Dressler et al. 1990; Aragón-Salamanca et al. 2003; Rakos & Schombert 1995; van der Marel & van Dokkum 2007; Cool et al. 2008; Whiley et al. 2008). Ellis et al. (1997), Stanford et al. (1998) and Blakeslee et al. (2003) showed that early-type galaxies in clusters at  $z \sim 0.5 - 1.2$  complete their star formation by  $z \geq 3$  (see also Ferreras et al. 1999; Gladders et al. 1998; Kodama et al. 1998; Nelson et al. 2001; van Dokkum et al. 2000). The same can be said for the most massive early-type galaxies ( $M_* > 10^{11}M_{\odot}$ ) in the field at the same redshift, while the less massive ones appear to sustain a more prolonged star formation (see e.g. Bell et al. 2004; van der Wel et al. 2004, 2005; van Dokkum & Ellis 2003; Treu et al. 2005a,b).

Although photometric colours and SEDs are clearly the most affordable observables to obtain in terms of telescope time, they do not disentangle between age and metallicity effects as accurately as spectra and line indices. The measurement of the  $Mgb$  index and of the  $H_{\delta}$  and  $H_{\gamma}$  strength in early-type galaxies up to  $z=0.83$  has independently provided  $z > 2 - 3$  as the redshift at which their stars formed (Ziegler & Bender 1997; Kelson et al. 2001). Spectroscopy from the ground has made also possible to use a set of FeII, MgII and MgI lines in the rest-frame UV and identify massive early-type galaxies ( $M_* > 10^{11}M_{\odot}$ ) up to  $z \simeq 2.15$  (Cimatti et al. 2004; Glazebrook et al. 2004; McCarthy et al. 2004; Saracco et al. 2005). In particular, Cimatti et al. (2004) stacked together the rest-frame UV spectra of 4 early-type galaxies with  $1.6 < z < 1.9$  and compared the average with synthetic spectra of simple stellar populations to find a mean stellar age of about 1 Gyr for solar metallicity (or better  $0.5 < \text{age} < 1.5$  Gyr for  $2.5 > Z/Z_{\odot} > 0.4$ ). Similarly, Cimatti et al. (2008) combined the spectra of 13 early-type galaxies at  $\langle z \rangle = 1.6$  and determined a mean stellar age in the range 0.7 - 2.8 Gyr for  $Z = 1.5 - 0.2Z_{\odot}$ , corresponding to a formation redshift  $z_F > 2$ . Along this line, Kriek et al. (2008) averaged the rest-frame optical spectra of 16 early-type galaxies at  $2 < z < 3$  to find the typical SED of a poststarburst galaxy with an age of about 1 Gyr for solar metallicity. They concluded that early-type galaxies are likely to form between  $z_F = 2$  and 3 and are not yet in place at  $z=3$  (see also Dunlop et al. 1996; Spinrad et al. 1997; Driver et al. 1998; Brammer & van Dokkum 2007; Kodama et al. 2007).

At redshifts  $z \gtrsim 1$ , though, the performances of ground-based spectrographs is severely limited by the atmosphere and its OH lines, and also by the optical faintness of the targets ( $I \gtrsim 23$  mag). The high-redshift population of early-type galaxies is, thus, best investigated from space with low-resolution spectroscopy. This is the case of the *HST* Advanced Camera for Surveys (ACS), which is equipped with a slitless grism covering the spectral range 5500 - 10500 Å with a dispersion of 40 Å/pix in the first spectral order (Pasquali et al. 2006a). The *HST*/ACS grism has been used for spectroscopic surveys like GRAPES (Pirzkal et al. 2004) and PEARS (Malhotra et al., in preparation), where early-type galaxies brighter than  $I \simeq 26$  mag have been identified up to  $z=2.5$  and their individual spectra (typically with  $S/N > 10$  pixel $^{-1}$ ) have been analyzed to constrain their stellar populations. The low resolution of these spectra clearly prevent us from measuring line indices, but allows us to detect the broad feature  $Mg_{UV}$  in the rest-frame 2640–2850 Å (Daddi et al. 2005; Maraston et al. 2006) at  $z > 1.3$  and measure the 4000Å break at  $0.4 < z < 1.2$  and use it along with the continuum to estimate stellar ages and metallicities down to  $M_* \simeq 10^9 - 10^{10}M_{\odot}$  (Pasquali et al. 2006b). This limiting stellar mass is a factor of about 10 lower than what can be achieved with ground-based spectroscopy, and makes it possible, for the first time, to study the stellar populations at the faint end of the red sequence at  $z \sim 1$ . For example, Pasquali et al. (2006b) identified 18 early-types in the Hubble Ultra Deep Field (Beckwith et al. 2006) with  $0.49 \leq z \leq 1.15$ . They fitted the individual *HST*/ACS grism spectra with synthetic star formation histories, based on the models

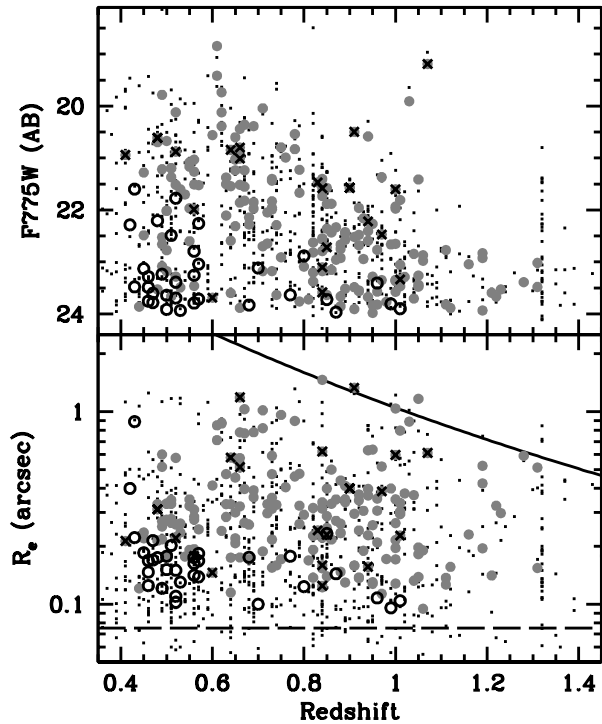


FIG. 1.— Observed properties of the PEARS early-type galaxy sample, extracted from visual classification in GOODS N and S *HST*/ACS images down to  $i_{AB} = 24$  mag (full sample shown as dots, Ferreras et al. 2009a). We cross-correlate the total sample of 377 (CDFs) and 533 (HDFN) early-types with the PEARS extractions. After visual rejection of bad spectra and rejection of redshifts  $z < 0.4$  we end up with the sample presented in this figure (circles): 91+13 (CDFs) and 104+20 (HDFN) galaxies. The first number represents those with a “red” SED (grey filled circles): prominent 4000-break and no emission lines. The second number corresponds to “blue” SEDs (open circles, see text for details). We overlay an ‘X’ symbol on those galaxies with an X-ray detection from the *Chandra* deep fields (Alexander et al. 2003; Luo et al. 2008). Notice that all X-ray detections correspond to “red” galaxies. The dashed line in the bottom panel illustrates the resolution limit at  $2R_e \sim \text{FWHM}_{\text{HST/ACS}}$ . The solid line is the surface brightness limit, considering the cosmological dimming, at  $i_{AB} = 24$  mag (AB), assuming a surface brightness at  $z=0.7$  of  $\mu_{\text{F775W}} = 22$  mag/arcsec<sup>2</sup>.

of Bruzual & Charlot (2003) and including chemical enrichment (Ferreras & Silk 2003). They found stellar ages varying from 3–4 Gyr at  $z > 0.65$  to 5–6 Gyr at lower redshifts, stellar metallicities between 1 and 0.03  $Z_{\odot}$  and stellar masses between  $3 \times 10^9$  and  $3 \times 10^{11} M_{\odot}$ . The estimated ages are consistent with a formation redshift  $z > 2-5$ .

In this paper, we extend the analysis of Pasquali et al. (2006b) to a sample of early-type galaxies that is a factor of 11 larger than in the HUDF. The objects – 228 in total – are extracted from the sample of morphologically selected early-type galaxies of Ferreras et al. (2009a) in the GOODS North and South fields and have been observed as part of PEARS<sup>1</sup>. This is the largest database of individual, high S/N grism spectra obtained so far for early-type galaxies at  $z \sim 1$ , that allows a study of their stellar populations as a function of

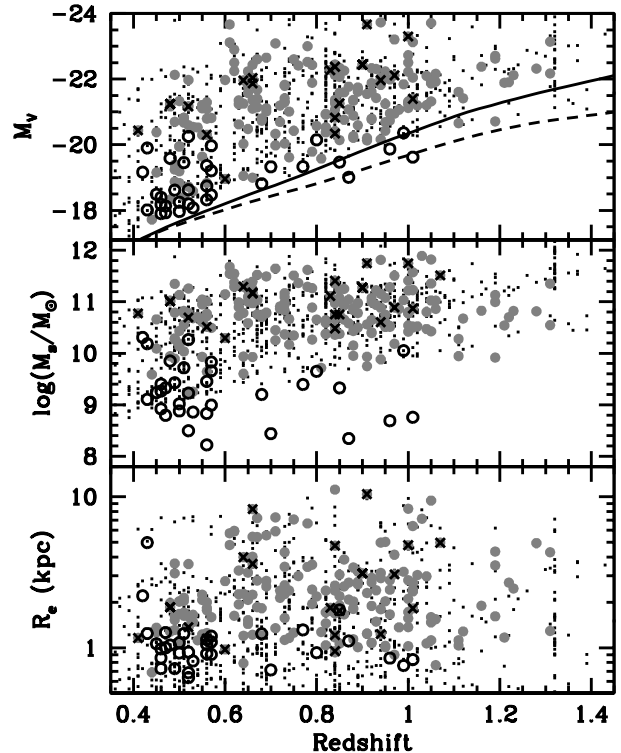


FIG. 2.— Rest-frame properties of PEARS early-type galaxies. The sample is shown with respect to absolute V-band magnitude (top), stellar mass (middle) and projected half-light radius (bottom). The masses and magnitudes are computed using the best-fit SFH. ‘Red’ and ‘blue’ galaxies are represented by filled and open circles, respectively. The solid lines at the top panel track the  $i_{AB} = 24$  mag cut in apparent magnitude for two extreme cases: an old, passively evolving population (solid) or an extended star formation history (dashed). The small dots correspond to the original sample of visually-classified spheroidal galaxies from Ferreras et al. (2009a). We overlay an ‘X’ symbol on those galaxies with an X-ray detection from the *Chandra* deep fields North and South (Alexander et al. 2003; Luo et al. 2008).

stellar mass and redshift, and can place more stringent constraints on the formation and evolution of (not only massive) early type galaxies since  $z \sim 1$ .

Throughout this paper a standard  $\Lambda$ CDM cosmology from the WMAP-year 5 data is used to determine ages and rest-frame properties (Komatsu et al. 2009).

## 2. COLLECTING THE SAMPLE OF EARLY-TYPE GALAXIES

The data consist of ACS images taken with the WFC G800L grism. The PEARS survey comprises eight pointings towards the GOODS North and South fields – 4 pointings each – with three *HST* roll angles for each pointing (20 *HST* orbits per field), plus the HUDF with four roll angles (40 *HST* orbits). A forthcoming paper (Malhotra et al. 2009, in preparation) will describe the PEARS project and data in detail. The HUDF data comes from an earlier similar project, GRAPES (Pirzkal et al. 2004; Pasquali et al. 2006b). We use the PEARS IDs from the master catalogue of source extractions. The G800L grism produces slitless, low-resolution spectra in the wavelength range 6000–9500Å. The optimal spectral resolution ( $R \sim 100$ ) is achieved for unresolved sources, whereas for our sample of early-type galaxies, the effec-

<sup>1</sup> <http://archive.stsci.edu/prepds/pears/>

TABLE 1  
CATALOG OF PEARS EARLY-TYPE GALAXIES: OBSERVED DATA

| PID <sup>a</sup> | RA<br>J2000, deg. | Dec        | F775W<br>(AB) | R <sub>e</sub><br>pix <sup>c</sup> | z    | R/B <sup>b</sup> |
|------------------|-------------------|------------|---------------|------------------------------------|------|------------------|
| 65620            | 53.1649933        | -27.819334 | 21.37         | 17.33                              | 0.97 | R                |
| 56798            | 189.1671143       | +62.218311 | 20.70         | 11.04                              | 0.48 | R                |
| 83499            | 189.1973572       | +62.274567 | 21.57         | 13.30                              | 0.85 | R                |
| 75762            | 189.1127472       | +62.252712 | 21.23         | 15.86                              | 0.79 | R                |
| 61447            | 53.1852264        | -27.827837 | 23.10         | 4.16                               | 0.84 | R                |
| 127697           | 53.0613937        | -27.698137 | 22.53         | 7.25                               | 0.49 | R                |
| 52017            | 189.1557922       | +62.208328 | 23.35         | 3.78                               | 0.97 | R                |
| 61235            | 53.1881218        | -27.827766 | 22.87         | 6.35                               | 1.06 | R                |
| 69419            | 53.1323776        | -27.814238 | 22.91         | 5.72                               | 0.75 | R                |
| 40498            | 189.1528931       | +62.186619 | 23.72         | 7.77                               | 0.85 | B                |
| 47252            | 189.2056274       | +62.198719 | 23.41         | 3.60                               | 0.96 | B                |
| 42729            | 53.2094307        | -27.861725 | 23.79         | 5.44                               | 0.56 | B                |
| 17362            | 53.1624603        | -27.914028 | 22.49         | 6.72                               | 0.51 | B                |
| 57554            | 189.2057190       | +62.219887 | 22.21         | 5.83                               | 0.48 | B                |
| 119723           | 189.3504181       | +62.327610 | 22.89         | 4.12                               | 0.80 | B                |
| 53462            | 53.1896324        | -27.841940 | 22.79         | 5.84                               | 0.56 | B                |
| 107477           | 53.0674744        | -27.739756 | 22.29         | 13.32                              | 0.42 | B                |
| 104645           | 189.3910980       | +62.301193 | 23.78         | 5.66                               | 0.47 | B                |

NOTE. — A full version of table 1 is published in its entirety in the electronic edition of the *Astrophysical Journal*. A portion is shown here for guidance regarding its form and content.

<sup>a</sup>PEARS ID number.

<sup>b</sup>‘Red’ vs ‘Blue’ early-type (see text for details).

<sup>c</sup>1 pixel = 0.03 arcsec

tive resolution is lower, around  $R \sim 50$ .

The master catalogue of PEARS detections was cross-correlated with the sample of 910 visually-classified early-type galaxies in the GOODS North and South fields of Ferreras et al. (2009a). This sample completes the one presented previously in the CDFS field (Ferrerias et al. 2005). The selection consists of visual inspection (in all four ACS bands) of all source detections brighter than  $i_{F775W} < 24$  mag (AB) by four people, with two rounds of visual inspection for those galaxies that were harder to classify. No colour cuts or CAS-based selections were made, although the sample is consistent with the high concentration and low asymmetry expected in spheroidal galaxies with respect to later morphological types (Lisker et al., in preparation). Furthermore, the visually-classified sample comprises 80% of red, quiescent stellar populations. We believe visual inspection alone is much more efficient at selecting spheroidal galaxies, eliminating contamination from late-type galaxies or unresolved sources, and removing the bias inherent in color-based selection methods. From this catalogue we extract the available PEARS spectra of each identified object from our database. The spectra are background corrected and scaled to match the direct image magnitudes of each object. Each file contains the spectra extracted for the different PAs (typically around three PAs per galaxy). We compute a simple average of the spectra available for each object, possibly excluding those PAs whose spectra are clearly deviant. The errors in the final combined spectra are computed by propagating the flux errors in each individual SED. The spectra were visually inspected, and some of them had to be discarded because of a very low signal-to-noise ratio, contamination from nearby sources, or because they were located close to the edge of the field. Out of the original sample of 910 galaxies (533 in HDFN and 377 in CDFS) we ex-

tracted 136 spectra in the North and 131 in the South. The number of rejected galaxies is 19 and 18 in the North and South fields, respectively.

Regarding redshift, we start with estimates from the PEARS-based general catalog of photometric redshifts (Cohen et al. in preparation), and the photometric redshift catalogue of Mobasher et al. (2004) and Ferreras et al. (2009a). Spectroscopic redshifts are available from FORS2 (Vanzella et al. 2008) and the VIRMOS-VLT Deep Survey (VVDS, Popesso et al. 2008) in the South, and from the Team Keck Redshift Survey (TKRS, Wirth et al. 2004) in the North. However, our slitless grism data has enough S/N to allow for an estimate of the redshifts *directly* from the low-resolution spectra. Two of us (I.F. and A.P.) inspected visually each SED and compared it with a number of template spectra to determine a rough estimate of the redshift. Then we ran a simple code that uses the guess and templates to accurately determine the redshift via a standard maximum likelihood method. The accuracy of our redshifts is as good as spectroscopic estimates for most of the galaxies, especially those with a prominent 4000Å break (i.e. the majority of the sample) or those with emission lines. Incidentally, some of our (grism-based) redshift estimates *improved* on the spectroscopic values from pipeline-processed databases such as GOODS/FORS2. This improvement is to be expected for the faintest galaxies with a quiescent spectra. In those cases the continuum from the ground-based spectroscopic data is very noisy and, simply put, our low-resolution spectra yield more photons per pixel over the CCD, significantly improving the signal. Hence, we consider our quoted redshifts as spectroscopically accurate.

Finally, we apply a cut in redshift, removing from the analysis all galaxies with redshift  $z < 0.4$ . At those redshifts the 4000Å break – on which the modelling strongly

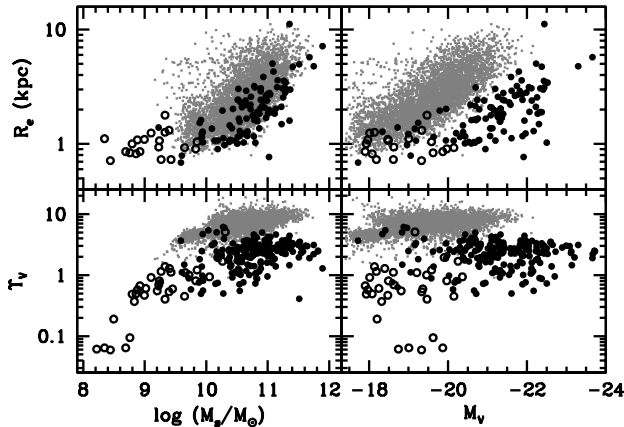


FIG. 3.— Comparison of half-light radius ( $R_e$ ; *top*) and  $V$ -band M/L ( $\Upsilon_V$  with respect to the solar value; *bottom*) with a  $z \sim 0$  sample of galaxies with Sersic index  $n_S > 2.5$ , extracted from the SDSS NYU Value Added Galaxy Catalogue (grey dots, Blanton et al. 2005). The half-light radius (*top*) and M/L in the  $V$  band is shown as a function of stellar mass (*left*) or absolute magnitude. ‘Red’ (‘blue’) PEARS galaxies are represented as black solid (open) circles.

relies – falls outside of the sensitivity region of the G800L grism. This cut reduces the sample to 124 and 104 galaxies in the North and South fields, bringing the total to 228 early-type galaxies with  $z > 0.4$  and  $i_{F775W} < 24$  mag (AB). The median redshift of the sample is  $z_M = 0.75$ . If we measure the signal-to-noise ratio as the average S/N per pixel within the spectral window 8000–8500Å, our sample has a median value of  $S/N \sim 15$  per pixel.

### 2.1. Sample Properties

The main observational data are presented in table 1. Figure 1 shows the distribution of total apparent magnitude (*top*) and size (half-light radius; *bottom*). The original sample of visually-classified galaxies from Ferreras et al. (2009a) is shown as small dots. The PEARS sample of early-type galaxies is shown as circles. We subdivide the sample into ‘red’ (grey dots) and ‘blue’ types (open circles). This classification is taken from the original data and is determined by the spectral template that gives the best fit in the analysis of photometric redshifts. For the PEARS sample presented here, the division is much more accurate because this information is complemented by the visual appearance of the low-resolution SED. ‘Red’ galaxies feature prominent 4000Å breaks, whereas ‘blue’ galaxies have a clear blue continuum with the occasional presence of emission lines. The sample comprises 195 ‘red’ and 33 ‘blue’ spheroidal galaxies. The accuracy of the total magnitudes and half-light radii is estimated from simulations of synthetic galaxies with Sersic profiles with similar values of size and magnitude as the original sample. We recover the original values with an uncertainty  $\Delta i_{F775W} = 0.05$  mag and  $\Delta R_e/R_e = 0.09$  (Ferreras et al. 2009a). We overlay ‘X’ symbols over those galaxies with an X-ray detection from the *Chandra* Deep fields North and South (Alexander et al. 2003; Luo et al. 2008). 22 sources have an X-ray detection which extends over the full range in apparent magnitude. It is worth emphasizing that all X-ray detected sources in our sample are photometrically classified as ‘red’ galaxies.

The distribution of rest-frame properties of our sam-

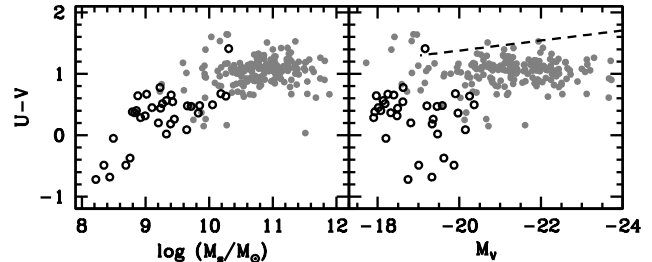


FIG. 4.— Rest-frame  $U-V$  color-magnitude relation (*right*) and color-stellar mass relation (*left*). Filled (open) circles correspond to photometric ‘red’ (‘blue’) galaxies. The dashed line gives the  $z \sim 0$  colour-magnitude relation of Coma early-type galaxies from Bower et al. (1992).

ple is shown in figure 2, where the absolute magnitude in the  $V$  band (*top*); stellar mass (*middle*) and physical half-light radius (*bottom*) is shown with respect to redshift. The K-correction and the M/L estimate needed for the top two panels is taken from the best fit models of the runs explained in §3. The ‘red’ (‘blue’) galaxies are shown as filled grey (open black) circles. ‘Blue’ early-types are mostly faint, low-mass galaxies. We should emphasize that our selection process (visual classification) does not introduce any bias regarding the color distribution. The lines in the top panel correspond to the  $i_{F775W} < 24$  mag limit imposed on the original sample. Since the translation from apparent to absolute magnitude depend on the template SED for the K-correction, we show the apparent magnitude limit corresponding to two types of populations: quiescent (solid line) and young (dashed line). These two cases are the extrema of the photometric types used in Ferreras et al. (2009a), namely  $t=0$  and  $t=7$ . These types correspond to an exponential star formation history at fixed solar metallicity, beginning at a formation redshift  $z_F = 3$  with timescale  $\tau = 0.05$  Gyr ( $t=0$ ) or  $\tau = 8$  Gyr ( $t=7$ ). Similarly to figure 1, the ‘X’ symbols are overlaid on those galaxies with an X-ray detection from the *Chandra* Deep Fields North and South (Alexander et al. 2003; Luo et al. 2008). Almost all X-ray detections correspond to galaxies brighter than  $M_V < -20$ , with stellar masses above  $10^{10} M_\odot$ . However, many of them are concentrated, with half-light radii  $R_e \sim 1$  kpc.

Figure 3 shows the physical half-light radius ( $R_e$ ; *top*) and M/L in the  $V$  band ( $\Upsilon_V$  with respect to the solar value; *bottom*) as a function of stellar mass (*left*) or absolute magnitude (*right*). Black filled (open) circles correspond to ‘red’ (‘blue’) galaxies. In order to compare with  $z=0$  galaxies, we include as grey dots the values from the DR4 NYU Value Added galaxy catalogue (Blanton et al. 2005) with a Sersic index  $n_S > 2.5$ . Local galaxies appear significantly larger and with higher M/L. The latter can be explained by pure passive evolution of the stellar populations, but the change in size requires a mechanism beyond stellar evolution. This result is shown for the full sample of GOODS spheroidal galaxies in Ferreras et al. (2009b) and confirms previous results at similar or higher redshifts (Trujillo et al. 2007). Size evolution is even stronger when galaxies at  $z \sim 2$  are considered (van Dokkum et al. 2008; Buitrago et al. 2008). Recent attempts at explaining the size evolution invoke

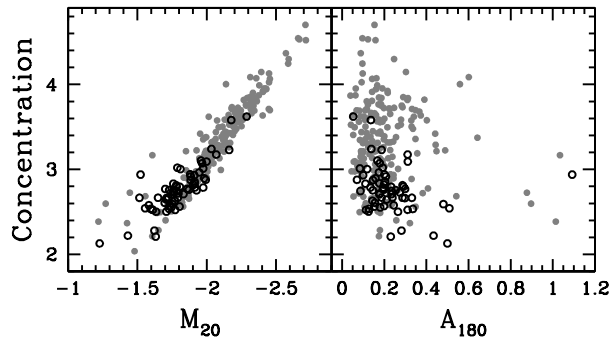


FIG. 5.— Quantitative morphology of the PEARS early-type galaxy sample. The plot shows the concentration,  $M_{20}$  (a normalized second order moment of the 20% brightest pixels) and asymmetry. Filled grey (black open) circles correspond to ‘red’ (‘blue’) spheroidal galaxies. See text for details.

a significant ejection of gas mass caused by quasar feedback (Fan et al. 2008), or via dry mergers in the standard paradigm of hierarchical evolution (Hopkins et al. 2009).

The rest-frame  $U-V$  color-magnitude and color-stellar mass relations are presented in figure 4, with the same coding for photometric type as in the previous figures. Notice color is correlated more strongly with stellar mass than with absolute magnitude. The dashed line gives the Coma color-magnitude relation from Bower et al. (1992) for E+S0s. The extent of the line covers the magnitude range probed in Coma. The relation at high redshift is in good agreement with Coma if we consider that passive evolution of a stellar population with solar metallicity, formed at  $z_F = 3$  changes its  $U-V$  colour by  $\sim 0.3$  mag between the median redshift of our sample  $\langle z \rangle \sim 0.7$  and  $z = 0$ . Instead of dealing with simple, K-corrected colors, we use the spectroscopic data to determine the best fit ages from models of stellar populations. In the next section we compare the low-resolution SEDs from PEARS with a large grid of star formation histories to transform this information into a more meaningful diagram involving stellar ages.

A rough morphological quantification of the sample is presented in figure 5, where the concentration,  $M_{20}$  and asymmetry values are shown for the  $i_{F775W}$  images (Lisker et al. in preparation). Concentration (see e.g. Bershady et al. 2000) is defined as  $C = 5 \log R_{80}/R_{20}$ , where  $R_X$  is defined as the radius within which the enclosed flux corresponds to X % of the total flux (as measured within the Petrosian radius).  $M_{20}$  is defined as the normalized second order moment of the brightest 20% of the pixels no matter where they are (Lotz et al. 2004). The asymmetry parameter ( $A_{180}$ ) is obtained by subtracting a  $180^\circ$  rotated image from the original.  $A_{180}$  is given by this difference – summed and expressed as a fraction of the original flux (Conselice 2003). The figure shows that most galaxies (whose selection was purely based on a visual classification, i.e. NOT extracted from their CAS values) are highly concentrated both in C and  $M_{20}$  and have low asymmetry. Notice the blue photometric types (open circles) coincide with the lowest values of concentration, although those values are still high for a general population involving all galaxy morphologies, which can have concentrations as low as  $C \sim 1.5$ . The

TABLE 2  
RANGE OF PARAMETERS EXPLORED FOR THE THREE MODELS  
CONSIDERED IN THIS PAPER (SEE TEXT FOR DETAILS).

| Model/Param                | MIN                      | MAX             | Comments              |
|----------------------------|--------------------------|-----------------|-----------------------|
| SSP                        |                          | 2 params        |                       |
| $t$                        | 0.1 Gyr                  | $z_F = 10^a$    | Age                   |
| $\log(Z/Z_\odot)$          | -1.5                     | +0.3            | Metallicity           |
| EXP                        |                          | 3 params        |                       |
| $\log \tau$ (Gyr)          | -1                       | +0.6            | Exp. Timescale        |
| $z_F$                      | $z-0.1$ Gyr <sup>b</sup> | 10              | Formation epoch       |
| $\log(Z/Z_\odot)$          | -1.5                     | +0.3            | Metallicity           |
| 2BST                       |                          | 4 params        |                       |
| $t_O$                      | 2                        | $z_F = 10^a$    | Old (Gyr)             |
| $t_Y$                      | 0.1                      | 2               | Young (Gyr)           |
| $f_Y$                      | 0.0                      | 1.0             | Mass fraction         |
| $\log(Z/Z_\odot)$          | -1.5                     | +0.3            | Metallicity           |
| CSP                        |                          | 3 (free) params |                       |
| $\nu$ (Gyr <sup>-1</sup> ) |                          | 20              | SF Efficiency (fixed) |
| $\tau_f$ (Gyr)             | -1                       | +0.3            | Gas Infall timescale  |
| $\beta$ (Gyr)              | 0                        | 1               | Outflow fraction      |
| $z_F$                      | $z-0.1$ Gyr <sup>a</sup> | 10              | Formation epoch       |

<sup>a</sup>SSP,2BST: The oldest age possible for the old component corresponds to a formation redshift  $z_F = 10$  at the redshift of the galaxy, e.g. 6.7 Gyr for a  $z=0.7$  galaxy.

<sup>b</sup>EXP,CSP: The latest formation redshift available corresponds to the observed redshift of the galaxy *minus* 0.1 Gyr, e.g.  $z_F > 0.72$  for a  $z=0.7$  galaxy.

asymmetry of blue and red early-types is similar.

### 3. MODELLING THE STAR FORMATION HISTORIES OF GALAXIES

Our slitless spectra have good enough S/N down to the  $i_{F775W} = 24$  mag (AB) limit of the original sample. The S/N ranges from 30 down to 4–5 per pixel at the limiting magnitude. One of the main advantages of G800L grism data for the analysis presented here is the superb flux calibration of the spectra enabled by the optimal flat fielding of the images. We estimate flux calibration systematic errors below 5% within the spectral range of interest (Pirzkal et al. 2004).

The wavelength coverage of the ACS/G800L grism (6000–9500Å) is ideally suited for the analysis of old stellar populations at  $z=0.4-1.5$ , because the prominent 4000Å break falls within its sensitivity range. Furthermore, the compact nature of early-type galaxies and their homogeneous stellar populations minimises the contamination and loss of spectral resolution compared to slitless grism data of late-type or irregular galaxies.

#### 3.1. Methodology

We follow a standard likelihood method fitting the low-resolution spectra to grids of models. A proper extraction of the age and metallicity distribution requires the use of composite models of stellar populations. Simple stellar populations (i.e. models with a single age and metallicity) will give luminosity-weighted age estimates that can differ significantly from a more physical mass-weighted age according to a composite stellar population (Ferreras & Yi 2004; Pasquali et al. 2005; Serra & Trager 2007; Rogers et al. 2008). In order to assess systematic differences related to the parameterisation of the star formation histories, we consider the following four models (whose parameters are summarised in table 2).

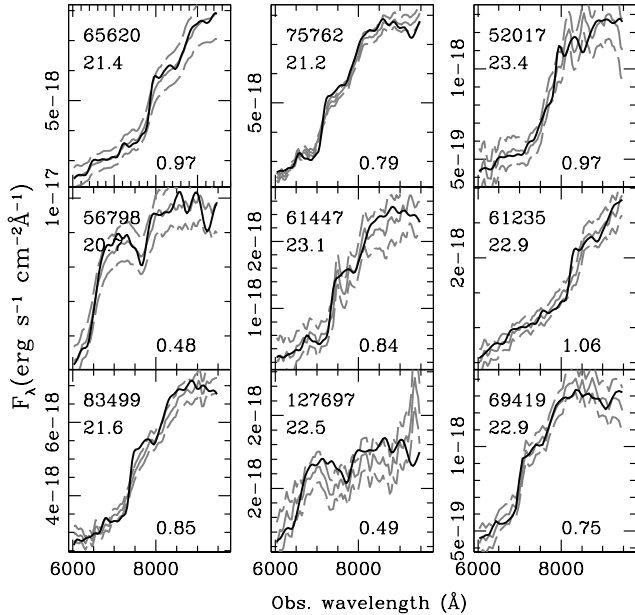


FIG. 6.— A sample of best fits to the grism data of ‘red’ early-type galaxies using models with chemical enrichment (CSP). Fits to the other two models considered in this paper (EXP and 2BST) do not differ much from these. The observed SEDs are shown in grey, including a  $1\sigma$  error envelopes (dashed lines). The model fits are shown as black solid lines. Each galaxy is labelled (from top to bottom) by their PEARS ID,  $i_{F775W}$  magnitude and redshift.

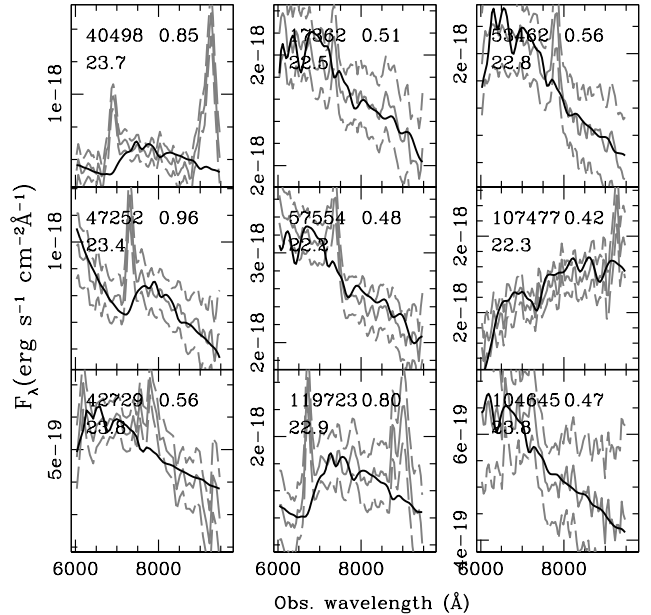


FIG. 7.— Same as figure 6 for a sample of ‘blue’ early-type galaxies. The fits also correspond to CSP models. In this case the fitting method excludes spectral windows of size  $\pm 100\text{\AA}$  around [O III], [O II],  $H\beta$ , and  $H\alpha$  lines whenever the redshift moves them into the spectral range of the grism data. (See Straughn et al. (2008) for details of emission line galaxies in the PEARS HUDF spectra).

- I. Simple Stellar Populations (SSP): SSPs are the building blocks of any population synthesis model. They correspond to a stellar population with a single age and metallicity. Although SSPs are often a fair approximation of a globular cluster, the longer timescales and more complex chemical enrichment history of a galaxy makes an SSP a very rough approximation in this case. Furthermore, the fact that a single age and metallicity are used to fit the data can introduce a significant difference between the SSP-determined age and a more physical mass-weighted age. Nevertheless, we include these models in the analysis for comparison, given that they are the simplest models from which the composite models are generated. This case explores a grid of  $128 \times 128$  SSPs over a wide range of ages and metallicities, as given in table 2.
- II.  $\tau$ -model (EXP): The SFH is described by an exponentially decaying function, with a timescale ( $\tau$ ) and a formation redshift ( $z_F$ ), corresponding to the epoch at which star formation starts. The metallicity is the third free parameter and it is kept constant throughout each SFH.
- III. 2-Burst (2BST): Superposition of two simple stellar populations, described by four parameters: the age of the old ( $t_O$ ) and the young components ( $t_Y$ ), the mass fraction in young stars ( $f_Y$ ) and the metallicity of the system (assumed to be the same for both populations).
- IV. Chemical Enrichment Model (CSP): We follow a consistent chemical enrichment code that incorporates the evolution of metallicity with the star for-

mation rate. The model is defined in Ferreras & Silk (2000) and was previously applied to similar data from the GRAPES sample of early-types and bulges in the HUDF (Pasquali et al. 2006b; Hathi et al. 2009). The formation history is described by four parameters: a star formation efficiency ( $\nu$ ) controlling the transformation of gas into stars via a Schmidt law; an outflow parameter ( $\beta$ ) which is the mass fraction of gas ejected as a result of the ongoing star formation rate; the exponential timescale of gas infall ( $\tau_f$ ); and the formation epoch given by the redshift ( $z_F$ ) at which infall starts.

For a given choice of parameters, the models determine the distribution of stellar ages and metallicities. These distributions are used to combine simple stellar populations from the latest 2007 models of Charlot & Bruzual (hereafter CB07, Bruzual & Charlot 2003; Bruzual 2007, latest models in preparation), assuming a Chabrier initial mass function (Chabrier 2003). Notice the CB07 models have been recently updated with respect to the high resolution spectra. However, at the low resolution grism spectra considered in this paper, the difference between CB07 and the expected CB09 models is negligible (Charlot, priv. comm.). The resulting spectra are degraded to the slitless PEARS SED, and compared via a standard maximum likelihood method. Each model is explored on a grid comprising between 32,000 and 65,000 realizations for a range of parameters as described in table 2. The best fit model is used to determine the age and metallicity of the underlying populations, and the M/L required to translate flux into stellar mass.

### 3.2. Extracting star formation histories

Figures 6 and 7 show some of the best fits of the CSP models for the ‘red’ and ‘blue’ galaxies, respectively. The model SED is shown as a solid black line, and the observed SED is shown in grey (including the  $1\sigma$  uncertainty as dashed lines). Notice ‘blue’ galaxies have emission lines, most notably [O II], [O III] and  $H\beta$ . These lines are masked out in the likelihood analysis. The blue spectra show a significant range of ages, from large  $4000\text{\AA}$  breaks (as in PID 119723) to very young stars (e.g. 47252). In this paper the analysis only deals with stellar populations, hence the presence of an AGN could significantly alter the estimated ages of the ‘blue’ galaxies. Nevertheless, figure 2 shows that the subsample of ‘blue’ galaxies is dominated by low-mass systems, for which one would expect a significant contribution to blue light from young stellar populations. One could argue that these low stellar mass estimates are biased because of the contribution from the AGN. However, the apparent magnitude of all ‘blue’ galaxies in our sample is consistently fainter than ‘red’ galaxies (see figure 1). The ‘red’ subsample (figure 6) looks much more homogeneous, with a prominent  $4000\text{\AA}$  break and no emission lines. The SEDs also display the characteristic dip around the G-band (rest-frame  $4300\text{\AA}$ ) and for the lower redshift galaxies one can also discern the Mg feature at rest-frame  $5170\text{\AA}$  (see e.g. PID 122743 or 127697 in figure 6). Needless to say, the low resolution of the G800L grism prevents us from doing any analysis of the absorption lines. However, the “smoothed-out” features of these spectra can contribute to constraining the age and metallicity distribution. Indeed, higher resolution spectra ( $R\sim 2000$ ) of Virgo elliptical galaxies at very high signal-to-noise ratio ( $S/N\gtrsim 100\text{\AA}^{-1}$ ) has shown that independent fits to the equivalent widths or a direct fit to the SED give age distributions that are in good agreement (Rogers et al. 2008).

#### 4. RESULTS AND CONCLUSIONS

Figure 8 shows the (mass-weighted) average age (top), age scatter (defined as an RMS, middle) and metallicity (bottom) as a function of stellar mass for three bins in redshift (top panel). These estimates correspond to the chemical enrichment models (CSP). The best fit star formation history from the models is used to compute the average and RMS of the age distribution. ‘Red’ and ‘blue’ early-types are shown as filled grey or open black circles, respectively. Characteristic error bars are included. The figure includes simple fits to the age distribution for the lowest redshift sample (black line in the top-left panel) and the highest redshift bin (black line in the top-right panel). The lines in grey are just copies of these two lines in the other panels, to guide the eye. The arrow in the top-right panel is the expected age difference between the high and the low redshift bin (i.e. pure passive evolution).

The figure allows us to understand the blue cloud-red sequence diagram of the sample. Our blue-cloud spheroidal galaxies are younger systems with roughly similar metallicities to the red sequence distribution. It is worth mentioning that the CSP models suggest all our galaxies have a similar *spread* of stellar ages, and it is only the *average* age that correlates with stellar mass. This result is consistent with the more detailed analysis of Rogers et al. (2008) on high-S/N spectra of ellip-

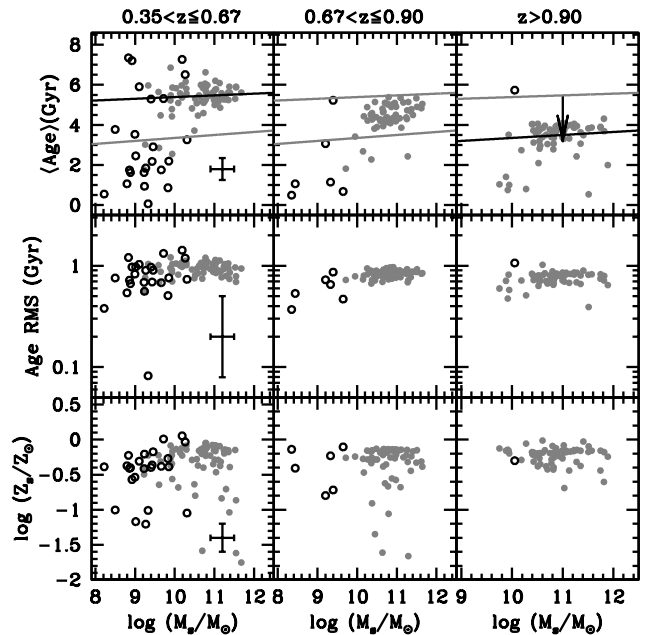


FIG. 8.— Best fit average age (top), age spread (middle, defined as the RMS of the distribution) and metallicity (bottom) for CSP models. The lines in the top panel are simple least square fits to the red galaxies for the lowest and highest redshift bins. These lines are shown in black for the subsamples where the fit was done. The grey lines are copies of these two fits, to guide the eye. The arrow in the top right panel corresponds to the lookback time between the median redshift of the high- and low redshift bins. On the left panels, characteristic error bars are shown. ‘Red’ (‘blue’) early-type galaxies are shown as grey filled (black open) circles.

tical galaxies in the Virgo cluster. The lines shown in the top panel illustrate that passive evolution over this redshift range can explain the ‘red’ spheroidals – which represent the large majority of the sample. The average ages of the subsample at lower redshift ( $0.35 \leq z \leq 0.67$ ; *top-left*) suggest that the correlation between stellar age and mass is such that instead of a monotonic trend, the scatter in age increases in galaxies with stellar masses below  $10^{10} M_{\odot}$  (see e.g. Caldwell et al. 2003; Gallazzi et al. 2006; Yamada et al. 2006; Rogers et al. 2008).

In order to check systematic effects arising from the specific way to parameterise the models, we compare in figure 9 the average age and metallicity distribution of the three models considered. There is overall good agreement between the CSP and the EXP models (top panels), whereas the age and metallicities of SSP and 2BST models differ significantly with respect to CSP models. Notice that best fit SSP metallicities are often very low, as the best fit wanders along the age-metallicity degeneracy, affecting the estimated ages. Composite models have been found to give more realistic metallicity constraints than SSPs (Ferreras & Yi 2004). However, we cannot look into the reduced  $\chi^2$  values to rule out one model against another: all models give equally acceptable values of  $\chi_r^2 \sim 1$ . Observations at higher spectral resolution do not fare better at disentangling this degeneracy (Rogers et al. 2008).

It is also worth mentioning that for the composite models (2BST, EXP and CSP) there is good agreement between the best-fit metallicities for the red galaxies – within a realistic  $\sim 0.3$  dex uncertainty. Blue galaxies, as

TABLE 3  
CATALOG OF PEARS EARLY-TYPE GALAXIES: PHYSICAL PROPERTIES (CSP MODELS)

| PID    | $M_s$<br>$\times 10^{10} M_\odot$ | $U - V$ | $M_V$  | $R_e$<br>kpc | $\langle t \rangle$<br>Gyr | $\sigma_t^a$<br>Gyr | $\langle \log Z/Z_\odot \rangle$ | $\beta$ | $z_F$ | $\log \tau$<br>Gyr |
|--------|-----------------------------------|---------|--------|--------------|----------------------------|---------------------|----------------------------------|---------|-------|--------------------|
| 65620  | 11.51                             | 1.06    | -23.20 | 4.13         | 3.82                       | 0.81                | -0.18                            | 0.28    | 7.5   | -0.48              |
| 56798  | 11.02                             | 1.28    | -21.17 | 1.98         | 6.21                       | 1.12                | -0.10                            | 0.21    | 9.8   | -0.31              |
| 83499  | 11.24                             | 1.05    | -22.34 | 3.06         | 4.40                       | 0.81                | -0.28                            | 0.37    | 7.5   | -0.56              |
| 75762  | 11.26                             | 1.24    | -22.43 | 3.56         | 4.73                       | 0.92                | -0.15                            | 0.24    | 9.9   | -0.35              |
| 61447  | 10.76                             | 1.14    | -20.83 | 0.95         | 4.39                       | 0.86                | -0.20                            | 0.32    | 7.6   | -0.47              |
| 127697 | 10.29                             | 1.17    | -19.39 | 1.31         | 5.81                       | 1.06                | -0.11                            | 0.17    | 5.5   | -0.53              |
| 52017  | 10.19                             | 0.80    | -20.95 | 0.90         | 2.71                       | 0.71                | -0.30                            | 0.41    | 3.2   | -0.50              |
| 61235  | 10.86                             | 1.06    | -22.16 | 1.55         | 3.64                       | 0.77                | -0.22                            | 0.33    | 9.8   | -0.48              |
| 69419  | 10.35                             | 1.08    | -20.42 | 1.26         | 4.51                       | 0.89                | -0.18                            | 0.26    | 6.0   | -0.48              |
| 40498  | 9.33                              | 0.02    | -19.47 | 1.79         | 1.05                       | 0.53                | -0.36                            | 0.45    | 0.8   | -0.07              |
| 47252  | 8.69                              | -0.49   | -19.87 | 0.86         | 0.10                       | 0.04                | -0.94                            | 0.41    | 0.9   | -0.26              |
| 42729  | 8.83                              | 0.37    | -18.32 | 1.06         | 0.66                       | 0.38                | -0.38                            | 0.45    | 0.7   | -0.12              |
| 17362  | 9.72                              | 0.47    | -19.45 | 1.24         | 2.35                       | 0.74                | -0.47                            | 0.58    | 1.2   | -0.22              |
| 57554  | 9.85                              | 0.48    | -19.58 | 1.04         | 1.98                       | 0.71                | -0.54                            | 0.61    | 1.0   | -0.19              |
| 119723 | 9.65                              | 0.09    | -20.15 | 0.93         | 0.65                       | 0.45                | -0.13                            | 0.20    | 1.1   | 0.10               |
| 53462  | 9.45                              | 0.26    | -19.36 | 1.13         | 0.92                       | 0.50                | -0.40                            | 0.48    | 1.0   | -0.04              |
| 107477 | 10.31                             | 1.41    | -19.16 | 2.21         | 2.27                       | 0.75                | -0.36                            | 0.46    | 1.0   | -0.22              |
| 104645 | 8.79                              | 0.38    | -17.93 | 1.00         | 0.95                       | 0.51                | -0.35                            | 0.44    | 0.6   | -0.07              |

NOTE. — A full version of table 3 is published in its entirety in the electronic edition of the *Astrophysical Journal*. A portion is shown here for guidance regarding its form and content.

<sup>a</sup> $\sigma_t$  is the root mean square of the stellar age distribution.

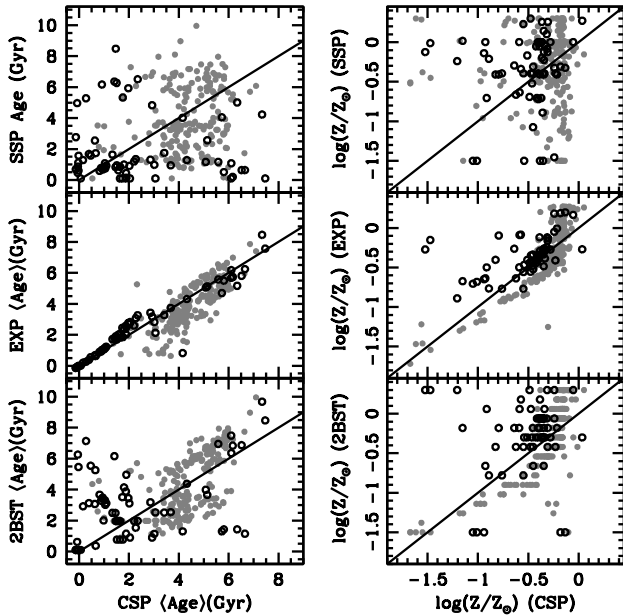


FIG. 9.— Comparison between the predicted average ages and metallicities for the models explored in this paper (see text for details). The solid line gives the 1:1 mapping. Solid (open) circles correspond to ‘red’ (‘blue’) early-type galaxies.

expected, give more discrepant results, mainly caused by the lack of spectral features in the low-resolution PEARS SEDs which makes metallicity estimates more uncertain.

Another check of our results was done with respect to the older version of the population synthesis models of Bruzual & Charlot (2003). In figure 10 we compare the average age and metallicity when using either the 2003 models (horizontal axes) or the improved CB07 models (vertical axes). The discrepancy between both versions is most prominent for the ‘blue’ subsample (open circles), which reflects the different treatment of some of

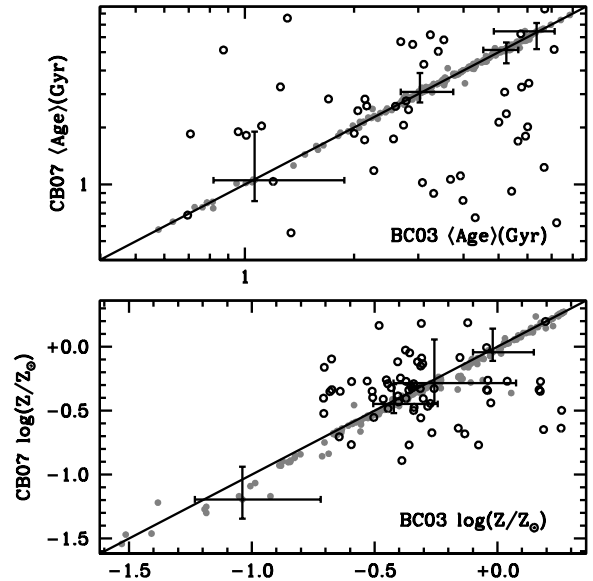


FIG. 10.— We illustrate here the effect of a different choice of stellar population models. The average age (*top*) and metallicity (*bottom*) of our models, based on the latest Charlot & Bruzual (2007) models, is compared with the predictions when the previous version of population synthesis models are used (Bruzual & Charlot 2003). Notice ‘red’ galaxies (filled circles) give similar results, whereas the younger populations found in the ‘blue’ subsample (open circles) depend strongly on the choice of population models.

the young-intermediate age phases of stellar evolution. The difference of age or metallicity between BC03 and CB07 models for older populations (‘red’ galaxies, grey circles) is negligible within the error bars.

The average and spread of the age distribution shown in figure 8 can be shown with respect to the phenomenological parameters used to describe the star formation

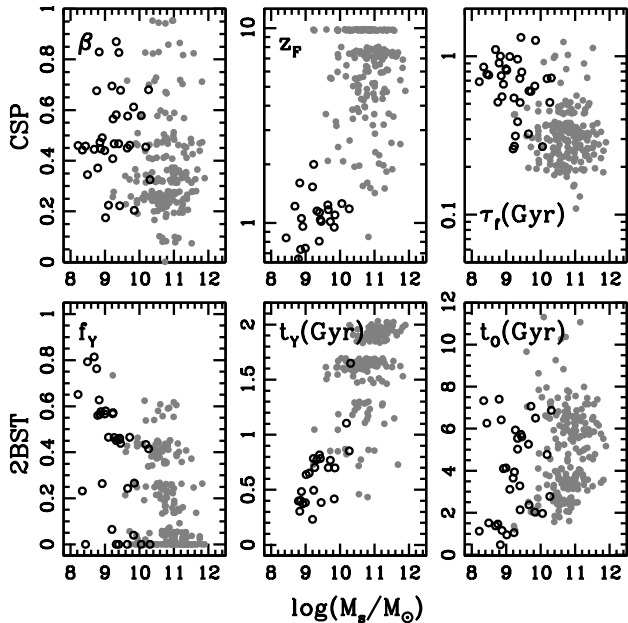


FIG. 11.— Best-fit parameters for a continuous model including chemical enrichment (CSP, top) or a two-burst scenario (2BST, bottom). The CSP parameters are (from left to right), the outflow fraction ( $\beta$ ), formation epoch ( $z_F$ ; defined as the time when gas infall starts) and the exponential timescale of gas infall ( $\tau_f$ ). The 2BST parameters are (also from left to right) the mass fraction in young stars ( $f_Y$ ); young stellar age ( $t_Y$ ); and old stellar age ( $t_O$ ).

history. Figure 11 shows the best-fit parameters for the CSP (top) and the 2BST (bottom) models as a function of stellar mass. A large spread is found for the fraction of gas and metals ejected in outflows ( $\beta$ ), whereas the gas infall timescale is overall rather short ( $\tau_f \lesssim 1$  Gyr). Over the  $0.4 < z < 1.2$  range probed by our sample – corresponding to a cosmic age between 5 and 10 Gyr (with 13.5 Gyr being our present age) – it is the formation epoch (top middle panel) what mainly correlates with stellar mass to give the age-mass trend shown in figure 8. Our ‘blue’ early-types have formation epochs  $z_F \sim 1$ , which – given the redshift of the sample – imply a large amount of young stars.

If we consider instead a two-burst model (2BST; bottom panels), the main driver of the age-mass relation is given by the young stellar mass fraction ( $t_Y$ ), although the mass fraction in young stars ( $f_Y$ ) also shows a correlation with mass. ‘Blue’ early-types have high values of  $f_Y$ . In general, we find that significant masses in young stars (open circles) only appear in early-type galaxies with masses  $\lesssim 10^{10} M_\odot$ . However, notice there is a fraction of ‘red’ early-type galaxies – which live on the red sequence (figure 4) – with a significant amount of young stars ( $f_Y \gtrsim 0.4$ ). This is consistent with the observed increase of the recent star formation in spheroidal galaxies with redshift (Kaviraj et al. 2008).

Both a smooth description of the star formation history (CSP) and a more abrupt model (2BST) confirm that red-sequence spheroidal galaxies with masses above  $\sim 10^{11} M_\odot$  have the bulk of their stellar populations formed at  $z_F \gtrsim 3$ . This result confirms previous findings (see e.g. Tantaló et al. 1996; Vazdekis et al. 1997; Pérez-González et al. 2008; Wiklind et al. 2008; Mancini et

al. 2009) although our work improves on the analysis, since we use SEDs instead of photometry to constrain the age distribution, and we consider a large volume of parameter space to describe the star formation history.

The old populations found in massive early-type galaxies in combination with the lack of number density evolution (see e.g. Ferreras et al. 2009b) confirms that new channels must be involved to explain the presence of galaxies on the red sequence at the massive end. In analogy to the cartoon version of the galaxy evolution tracks A-C in figure 10 of Faber et al. (2007), we propose a new one (track D) in the right panel of our figure 12. Tracks A-C (left panel) follow the standard growth via wet mergers on the blue cloud, followed by quenching of star formation (the near vertical black arrow) after which growth to the top of the red sequence consists of dry mergers (white arrow). This option is still controversial, since different semi-analytic models predict a very different redshift evolution of the number density (Ferrerias et al. 2009b, Hopkins et al., in preparation). On the other hand, the recent work of Dekel et al. (2009) based on the Mare Nostrum cosmological simulations suggest a significant amount of massive galaxy growth via cold accretion at the intersection of cosmic filaments. This process would bypass the evolution in the blue cloud, as visualised by our track D on the right panel of figure 12. In this case, most of the stellar component in a massive galaxy would grow *in situ*, over a short and early period, explaining the old populations found in massive galaxies (i.e. the ‘explosion’ symbol in our track D). Furthermore, this process would be very efficient, turning gas into stars over short timescales, thereby explaining the small infall timescales found (figure 11). The fact that formation epoch correlates with stellar mass would indicate the connection between the stellar mass of the galaxy and the significance of the overdensity from which these galaxies grow. Lower masses correspond to ‘lower- $\sigma$ ’ fluctuations thereby collapsing later. Nevertheless, it is worth emphasizing that the channel proposed by Dekel et al. (2009) would dominate at the most massive end. Intermediate mass galaxies will have a more complex history, with both tracks A-C and D contributing to their formation. The picture is unfortunately not fully explained, as massive galaxies also experience a very significant size evolution between  $z \sim 2$  and  $z = 0$  (Daddi et al. 2005; van Dokkum et al. 2008; Buitrago et al. 2008), an issue not explained yet in the context of Dekel et al. (2009).

As a final note, we may speculate on the importance of the formation redshifts shown in the top-middle panel of figure 11. The best-fit values range between  $z_F \simeq 0.5$  to  $z_F \sim 10$ , as expected in hierarchical formation scenarios that produce a broad peak in the cosmic SFH at  $z \sim 1-2$ . However, we also note that the highest formation redshifts pile up either between  $z_F \simeq 7-8$  or around  $z_F \simeq 10$ . While the estimates of the current spectrophotometry and SED modelling is undoubtedly not accurate enough to state the difference between the epochs  $z_F \simeq 7-8$  and  $z_F \simeq 10$  with any great confidence, it is tempting to notice that these redshifts coincide remarkably well with the epochs in WMAP-year5 cosmology where the peak of the Pop III star-formation should have occurred at  $z \simeq 10.8 \pm 1.8$  in order to produce the WMAP-year5 polarization optical depth (Dunkley et al. 2009), and with the

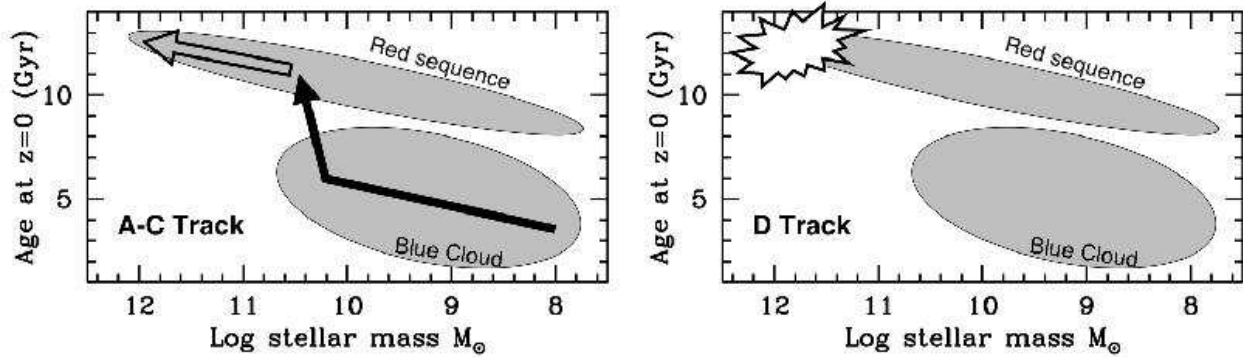


FIG. 12.— Our proposed additional channel for the formation of galaxies on the red sequence is shown as ‘D track’ (right), in comparison with the standard picture from Faber et al. (2007) (A-C track, left). The age distribution of our sample of moderate redshift early-type galaxies along with recent findings of a lack of evolution of the comoving number density or the intrinsic colour distribution of massive galaxies (see e.g. Fontana et al. 2006; Conselice et al. 2007; Ferreras et al. 2009b) suggest an *in situ* build-up of the stellar populations bypassing any trajectory in the blue cloud (except for the very short-lived formation stage corresponding to an intense, highly efficient process of star formation). This proposed channel can be justified by the cold accretion streams found in recent numerical simulations (Dekel et al. 2009).

epoch of  $z_F \simeq 7-8$  in which the global component of Pop II stars should have started shining in dwarf galaxies in order to finish reionization by  $z \simeq 6$ . Future data and modeling should concentrate on whether these epochs can be defined any more accurately than possible here. This analysis may be feasible with the upcoming HST/WFC3 grism spectra of the earliest type galaxies at  $1 \leq z \leq 3$  in the near future.

We would like to thank Stéphane Charlot for mak-

ing available the latest Charlot & Bruzual population synthesis models. The anonymous referee is gratefully acknowledged for useful comments. The project presented in this paper made use of the UCL High Performance Computing facility Legion. This research was supported in part by grants HST-GO-10530 and HST-GO-9793 from STScI, which is operated by AURA for NASA under contract NAS 5-26555.

Facilities: *HST* (ACS)

#### REFERENCES

- Alexander, D. M., et al. 2003, *AJ*, 126, 539  
Aragón-Salamanca, A., Ellis, R. S., Couch, W. J. & Carter, D. 1993, *MNRAS*, 262, 764  
Beckwith, S. V. W., et al. 2006, *AJ*, 132, 1729  
Bell, E. F. et al. 2004, *ApJ*, 608, 752  
Bershady, M. A., Jangren, A. & Conselice, C. J. 2000, *AJ*, 119, 2645  
Bernardi, M., et al. 2003, *AJ*, 125, 1882  
Blakeslee, J. P., et al. 2003, *ApJ*, 596, 143  
Blanton, M. R., et al. 2003, *ApJ*, 594, 186  
Blanton, M. R., et al. 2005, *AJ*, 129, 2562  
Borch, A., et al. 2006, *A&A*, 453, 869  
Bower, R. G., Lucey, J. R. & Ellis, R. S. 1992, *MNRAS*, 254, 601  
Brammer, G. B. & van Dokkum, P. G. 2007, *ApJ*, 654, 107  
Bruzual, G. & Charlot, S. 2003, *MNRAS*, 344, 1000  
Bruzual, G. 2007, IAU No. 241 Symp. Procs. “Stellar populations as building blocks of galaxies”, eds. A. Vazdekis and R. F. Peletier, Cambridge, arXiv:astro-ph/0703052  
Buitrago, F., Trujillo, I., Conselice, C., Bouwens, R. J., Dickinson, M. & Yan, H., 2008, *ApJ*, 687, L61  
Caldwell, N., Rose, J. A. & Concannon, K. D. 2003, *AJ*, 125, 2891  
Cappellari, M., et al. , 2009, arXiv:0906.3648  
Chabrier, G. 2003, *PASP*, 15, 763  
Cenarro, J. & Trujillo, I. 2009, *ApJ*, 696, L43  
Cimatti, A., et al. 2004, *Nature*, 430, 184  
Cimatti, A., et al. 2008, *A&A*, 482, 21  
Conselice, C. J. 2003, *ApJS*, 147, 1  
Conselice, C. J., et al. 2007, *MNRAS*, 381, 962  
Cool, R. J., et al. 2008, *ApJ*, 682, 919  
Croton, D. J., et al. 2005, *MNRAS*, 356, 1155  
Croton, D. J., et al. 2006, *MNRAS*, 365, 11  
Daddi, E., et al. 2005, *ApJ*, 626, 680  
Dekel, A., et al. 2009, *Nature*, 457, 451  
De Lucia, G., Springel, V., White, S. D. M., Croton, D. & Kauffmann, G. 2006, *MNRAS*, 366, 499  
Dressler, A., Gunn, J.E., 1990, *ASPC*, 10, 200  
Driver, S. P., Fernández-Soto, A., Couch, W. J., Odewahn, S. C., Windhorst, R. A., Phillips, S., Lanzetta, K. & Yahil, A. 1998, *ApJ*, 496, L93  
Dunkley, J., et al. 2009, *ApJS*, 180, 306  
Dunlop, J., Peacock, J., Spinrad, H., Dey, A., Jimenez, R., Stern, D. & Windhorst, R. 1996, *Nature*, 381, 581  
Eggen, O. J., Lynden-Bell, D. & Sandage, A. R. 1962, *ApJ*, 136, 748  
Ellis, R. S., Smail, I., Dressler, A., Couch, W. J., Oemler, A. Jr., Butcher, H. & Sharples, R. M. 1997, *ApJ*, 483, 582  
Faber, S. M., et al. 2007, *AJ*, 665, 265  
Fan, L., Lapi, A., De Zotti, G. & Danese, L. 2008, *ApJ*, 689, L101  
Ferreras, I., Charlot, S. & Silk, J. 1999, *ApJ*, 521, 81  
Ferreras, I. & Silk, J. 2000, *ApJ*, 532, 193  
Ferreras, I. & Silk, J. 2003, *MNRAS*, 344, 455  
Ferreras, I. & Yi, S. K. 2004, *MNRAS*, 350, 1322  
Ferreras, I., Lisker, T., Carollo, C. M., Lilly, S. J. & Mobasher, B. 2005, *ApJ*, 635, 243  
Ferreras, I., Pasquali, A., de Carvalho, R. R., de la Rosa, I. G. & Lahav, O. 2006, *MNRAS*, 370, 828  
Ferreras, I., Lisker, T., Pasquali, A. & Kaviraj, S., 2009a, *MNRAS*, 395, 554  
Ferreras, I., Lisker, T., Pasquali, A., Khochfar, S. & Kaviraj, S. 2009b, *MNRAS*, 396, 1573  
Fontana, A., et al. 2006, *A&A*, 459, 745  
Gallazzi, A., Charlot, S., Brichmann, J. & White, S. D. M. 2008, *MNRAS*, 387, 1253  
Gladders, M. D., Lopez-Cruz, O., Yee, H. K. C. & Kodama, T. 1998, *ApJ*, 501, 571  
Glazebrook, K., et al. 2004, *Nature*, 430, 181  
Hathi, N. P., Ferreras, I., Pasquali, A., Malhotra, S., Rhoads, J. E., Pirzkal, N., Windhorst, R. A. & Xu, C. 2009, *ApJ*, 690, 1866  
Hopkins, P. F., Somerville, R. S., Hernquist, L., Cox, T. J., Robertson, B. & Li, Y. 2006, *ApJ*, 652, 864  
Hopkins, P. F., Cox, T. J., Keres, D. & Hernquist, L. 2008, *ApJS*, 175, 390  
Hopkins, P. F., Hernquist, L., Cox, T. J., Keres, D. & Wuyts, S. 2009, *ApJ*, 691, 1424

- Hubble, E. D. 1926, *ApJ*, 64, 321
- Kaviraj, S., Devriendt, J. E. G., Ferreras, I. & Yi, S. K. 2005, *MNRAS*, 360, 60
- Kaviraj, S., et al. 2007, *ApJS*, 173, 619
- Kaviraj, S., et al. 2008, *MNRAS*, 388, 67
- Kelson, D. D., Illingworth, G. D., van Dokkum, P. G. & Franx, M. 2000, *ApJ*, 531, 184
- Kelson, D. D., Illingworth, G. D., Franx, M. & van Dokkum, P. G. 2001, *ApJ*, 552, 17
- Khochfar, S. & Silk, J. 2006a, *MNRAS*, 370, 902
- Khochfar, S. & Silk, J. 2006b, *ApJ*, 648, 21
- Kodama, T. & Arimoto, N. 1997, *A&A*, 320, 41
- Kodama, T., Arimoto, N., Barger, A. J. & Aragón-Salamanca, A. 1998, *A&A*, 334, 99
- Kodama, T., et al. 2007, *MNRAS*, 377, 1717
- Komatsu, E. et al. 2009, *ApJS*, 180, 330
- Kriek, M., van der Wel, A., van Dokkum, P. G., Franx, M. & Illingworth, G. D. 2008, *ApJ*, 682, 896
- Larson, R. B. 1974, *MNRAS*, 166, 585
- Lintott, C. J., Ferreras, I. & Lahav, O. 2006, *ApJ*, 648, 826
- Lotz, J. M., Primack, J. & Madau, P. 2004, *AJ*, 128, 163
- Luo, B., et al. 2008, *ApJS*, 179, 19
- Mancini, C., Matute, I., Cimatti, A., Daddi, E., Dickinson, M., Rodighiero, G., Bolzonella, M. & Pozzetti, L., 2009, *A&A*, in press, arXiv:0901.3341
- Maraston, C., et al. 2006, *ApJ*, 652, 85
- McCarthy, P. J., et al. 2004, *ApJ*, 614, 9
- McIntosh, D. H., et al. 2005, *ApJ*, 632, 191
- Mobasher, B., et al. 2004, *ApJ*, 600, L167
- Monaco, P., Fontanot, F. & Taffoni, G. 2007, *MNRAS*, 375, 1189
- Nelan, J. E., et al. 2005, *ApJ*, 632, 137
- Nelson, A. E., González, A. H., Zaritsky, D. & Dalcanton, J. J. 2001, *ApJ*, 563, 629
- Pasquali, A., Larsen, S., Ferreras, I., Gnedin, O. Y., Malhotra, S., Rhoads, J. E., Pirzkal, N. & Walsh, J. R. 2005, *AJ*, 129, 148
- Pasquali, A., Pirzkal, N., Larsen, S., Walsh, J. R. & Kümmel, M. 2006a, *PASP*, 118, 270
- Pasquali, A., et al. 2006b, *ApJ*, 636, 115
- Pérez-González, P. G., et al. 2008, *ApJ*, 675, 234
- Pirzkal, N., et al. 2004, *ApJS*, 154, 501
- Popesso, P., et al. 2008, *A&A*, submitted, arXiv:0802.2930
- Rakos, K. D. & Schombert, J. M., 1995, *ApJ*, 439, 47
- Rogers, B., Ferreras, I., Lahav, O., Bernardi, M., Kaviraj, S. & Yi, S. K. 2007, *MNRAS*, 382, 750
- Rogers, B., Ferreras, I., Peletier, R. F. & Silk, J. 2008, *MNRAS*, submitted, arXiv:0812.2029
- Saracco, P., et al. 2005, *MNRAS*, 357, 40
- Scannapieco, E., Silk, J. & Bouwens, R. 2005, *ApJ*, 635, L13
- Scarlata, C., et al. 2007, *ApJS*, 172, 494
- Schawinski, K., et al. 2007, *ApJS*, 173, 512
- Serra, P. & Trager, S. C. 2007, *MNRAS*, 374, 769
- Shen, S., Mo, H. J., White, S. D. M., Blanton, M. R., Kauffmann, G., Voges, W., Brinkmann, J. & Csabai, I. 2003, *MNRAS*, 343, 978
- Somerville, R. S., Hopkins, P. F., Cox, T. J., Robertson, B. E. & Hernquist, L. 2008, *MNRAS*, 391, 481
- Spinrad, H., Dey, A., Stern, D., Dunlop, J., Peacock, J., Jimenez, R. & Windhorst, R. 1997, *ApJ*, 484, 581
- Stanford, S. A., Eisenhardt, P. R., Dickinson, M. 1998, *ApJ*, 492, 461
- Strateva, I., et al. 2001, *AJ*, 122, 1861
- Straughn, A. et al. 2008, *AJ*, 135, 1624
- Tantalo, R., Chiosi, C., Bressan, A. & Fagotto, F. 1996, *A&A*, 311, 361
- Thomas, D., Greggio, L. & Bender, R. 1999, *MNRAS*, 302, 537
- Thomas, D., Maraston, C., Bender, R. & Mendes de Oliveira, C. 2005, *ApJ*, 621, 673
- Trager, S. C., Faber, S. M., Worthey, G. & González, J. J. 2000, *AJ*, 120, 165
- Treu, T., Ellis, R. S., Liao, T. X. & van Dokkum, P. G. 2005a, *ApJ*, 622, 5
- Treu, T., et al. 2005b, *ApJ*, 633, 174
- Trujillo, I., et al. 2006, *ApJ*, 650, 18
- Trujillo, I., Conselice, C. J., Bundy, K., Cooper, M. C., Eisenhardt, P. & Ellis, R. S. 2007, *MNRAS*, 382, 109
- Vanzella, E., et al. 2008, *A&A*, 478, 83
- Vazdekis, A., Peletier, R. F., Beckman, J. E. & Casuso, E. 1997, *ApJS*, 111, 203
- Vazdekis, A., Kuntschner, H., Davies, R. L., Arimoto, N., Nakamura, O. & Peletier, R. 2001, *ApJ*, 551, 127
- van der Marel, R. P. & van Dokkum, P. G. 2007, *ApJ*, 668, 756
- van der Wel, A., Franx, M., van Dokkum, P. G. & Rix, H.-W. 2004, *ApJ*, 601, 5
- van der Wel, A., Franx, M., van Dokkum, P. G., Rix, H.-W., Illingworth, G. D. & Rosati, P. 2005, *ApJ*, 631, 145
- van der Wel, A., Holden, B. P., Zirm, A. W., Franx, M., Rettura, A., Illingworth, G. D. & Ford, H. C. 2008, *ApJ*, 688, 48
- van Dokkum, P. G., Franx, M., Kelson, D. D. & Illingworth, G. D. 1998, *ApJ*, 504, 17
- van Dokkum, P. G., Franx, M., Fabricant, D., Illingworth, G. D. & Kelson, D. D. 2000, *ApJ*, 541, 951
- van Dokkum, P. G. & Ellis, R. S. 2003, *ApJ*, 592, 53
- van Dokkum, P. G., et al. 2008, *ApJ*, 677, L5
- van Dokkum, P. G., Kriek, M. & Franx, M. 2009, *Nature*, in press, arXiv:0906.2778
- Waddington, I., et al. 2002, *MNRAS*, 336, 1342
- Wiley, I. M., et al. 2008, *MNRAS*, 387, 1253
- Wiklund, T., Dickinson, M., Ferguson, H. C., Giavalisco, M., Mobasher, B., Grogin, N. A. & Panagia, N. 2008, *ApJ*, 676, 781
- Wirth, G., et al., 2004, *AJ*, 127, 3121
- Yamada, Y., Arimoto, N., Vazdekis, A. & Peletier, R. F. 2006, *ApJ*, 637, 200
- Ziegler, B. L. & Bender, R. 1997, *MNRAS*, 291, 527
- Ziegler, B. L., Saglia, R. P., Bender, R. & Belloni, P. 1999, *A&A*, 346, 13